# Spin-dependent plasma frequency from all-electron *ab initio* calculations including spin-orbit coupling

Maria K. Pogodaeva ⬤,[*] Sergey V. Levchenko, and Vladimir P. Drachev
*Skolkovo Institute of Science and Technology, Bolshoy Boulevard 30/1, Moscow 121205, Russia*

We present a first-principles methodology to calculate spin-dependent plasma frequency. Electronic structure and plasma frequency of nine metals (Al, Au, Ag, Cu, Pd, Pt, Na, Fe, and Co) are studied using density-functional theory in an all-electron full-potential framework. The results are compared to pseudopotential approaches and experiments. We find a significant difference between the spin-up and spin-down contributions to plasma frequency. Thus, spin-polarization effects are important for understanding optical properties of metals. Spin-orbit coupling inclusion affects plasma frequency since it contains an interaction term between spin-up and spin-down electrons.

## I. INTRODUCTION

There is no clear understanding of the effects of magnetization on plasma frequency so far. Our recent research in plasmonics has shown an inconsistency between theoretical predictions and experimental measurements of optical properties of cobalt nanoparticles [1]. Specifically, a plasmon resonance was observed at 280 nm for cobalt nanoparticles that could not be reproduced by permittivity measurements for large-area films (see Fig. 1).

The Mott model suggests that in magnetic metals there are two largely independent spin channels of conductivity. The probability of spin-flip scattering is low, and scattering rates for spin-up and spin-down channels are sufficiently different. The position of the absorption peak in the nanoparticles (Fig. 1) depends of the plasmon frequency $\omega_p$, which is proportional to bulk plasma frequency $\omega_{pl}$ [1]:

$$\omega_p^2 = \frac{\omega_{pl}^2}{\varepsilon_{ib} + 2\varepsilon_h}, \qquad (1)$$

where $\varepsilon_h$ is the dielectric permittivity of the host medium (hexane in Ref. [1]), and $\varepsilon_{ib}$ is the interband contribution to the metal permittivity.

Thus, separate consideration of spin channels for bulk plasma frequencies will allow us to make the first step toward understanding the unexpected plasmon resonances in magnetic nanoparticles, which the plasmonics currently fails to predict [1,2]. Spin-orbit coupling is also important since it contains an interaction term between electrons of opposite spins. However, to fully reproduce the absorption spectrum, the consideration of electronic relaxation times and optical interband transitions will be required.

Ground-state DFT is a powerful tool for calculating atomic and electronic structure of solids. Several studies have demonstrated that combining ground-state DFT with random-phase approximation is a computationally efficient way to model dielectric response of metals with an acceptable accuracy. Nevertheless, there is an inconsistency between computational results reported in the literature. In particular, several different values of plasma frequency are reported for gold: 8.59 eV (DFT-LDA [3–5]), 8.65 eV (PBE [6,7]), 9.0 eV (PBE, [8]), and 8.96 eV (PBE, [9]). The inclusion of spin-orbit coupling in the study [9] resulted in a decrease of plasma frequency from 8.96 eV to 8.81 eV. The results underestimate the experimental value of 9.1 eV [10].

For silver, DFT-LDA calculations yield 9.38 eV [5] and 9.48 eV [11], while for the PBE exchange-correlation functional the plasma frequency is 9.2 eV. Also, for silver nanoparticles an attempt to calculate the plasmon frequency has been made [12], and it was shown that the frequency increases with the nanoparticle radius and approaches bulk value for big nanoparticles. LDA slightly overestimates plasma frequency for silver compared to the experiment which is 9.2 eV [10]. For copper, the DFT-LDA values are 8.97 eV [5] and 9.27 eV [13]. The second value perfectly agrees with the value of 9.3 eV, experimentally derived by Johnson and Christy [10]. For aluminum, the PBE data on plasma frequency reported in the literature [8,14] is 12.6 eV, to be compared to experimentally derived value of 12.4 eV [15]. It is worth noting that originally the experiment was misinterpreted [16] because of a large interband contribution at low frequencies, demonstrating challenges in experimental determination of plasma frequency and the need for *ab initio* calculations. For sodium the experimental plasma frequency reported in the work [17] is 6.0 eV, which is in good agreement with the PBE result of 6.04 eV [8]. Also, studies of size-dependent optical properties for sodium clusters have been reported [18]. PBE [8] and experimental [2] plasma frequency for palladium are 7.4 eV.

Recently the experimental value of the plasma frequency of platinum [9] was questioned. Like aluminum, platinum has a large interband contribution at low frequencies, which makes Drude fitting and plasma frequency extraction challenging.
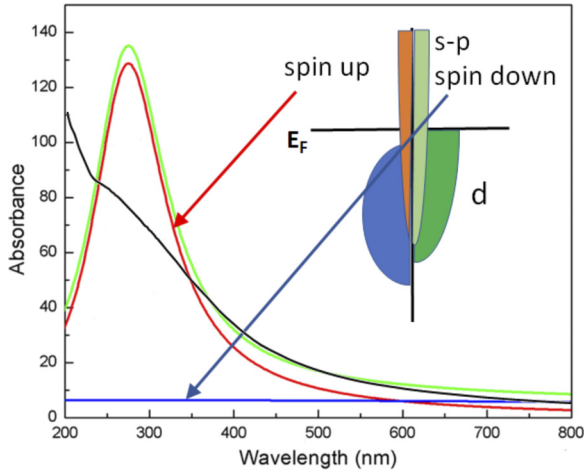
*mariia.pogodaeva@skoltech.ru

FIG. 1. Two-plasmon model for cobalt nanoparticle absorbance. Red line shows the contribution from spin-majority electrons, while blue line shows the contribution from spin-minority electrons. Green line shows the experimentally observed total spectrum. Black line shows theoretically predicted spectrum that does not consider different contributions from different spins [1] using data for bulk Co from [2]. Inset: a cartoon of projected density of states of cobalt.

Currently, the computed PBE value is 8.8 eV [8,9]. However, the inclusion of spin-orbit interaction resulted in a large decrease in the calculated plasma frequency to 7.54 eV. [9]

DFT results depend on the approximation to exchange-correlation functional. Alternatively, $GW$ approximation and the Bethe-Salpeter equation can be used to obtain accurate optical properties of solids [11]. In $GW$ approach electronic self-energy is expressed in terms of the single-particle Green's function $G$ and the screened Coulomb interaction $W$, which results in very accurate quasiparticle energies. The Bethe-Salpeter equation includes excitonic effects on top of $GW$. However, these methods are much more computationally expensive than DFT with standard approximations to the exchange-correlation functional.

In this paper, we use DFT with GGA and meta-GGA functionals to calculate a spin-dependent plasma frequency. We show that for magnetic metals plasma frequency varies significantly for spin-majority and spin-minority electrons. The PBE approximation is chosen since it is widely used for plasma frequency calculations [8,9,14], while SCAN has been shown to significantly improve over PBE [19] for many properties, as is confirmed by our own results presented below. We introduce a methodology to calculate plasma frequency in an all-electron full-potential framework using numeric atomic orbital basis sets. Using the localized basis will make future calculations of optical properties of low-dimensional systems (surfaces, nanowires, and nano-particles) more computationally efficient. The contributions to the plasma frequency from each spin channel are analyzed. *Ab initio* simulations allow us to identify different contributions to the spindependence of optical properties of metals and metal nanoparticles. To the best of our knowledge, no theoretical analysis of different spin-channel contributions to plasma frequency have been performed previously.

## II. IMPLEMENTATION

### A. Scalar-relativistic

As detailed in Refs. [8,14], plasma frequency can be calculated in the following way:

$$
\begin{aligned}
\bar{\omega}_{ij}^2 &= \bar{\omega}_{ij}^{\uparrow\,2} + \bar{\omega}_{ij}^{\downarrow\,2} \\
&= -\frac{4\pi}{V} \sum_{\sigma n \mathbf{k}} \frac{\partial f(\varepsilon_n^\sigma)}{\partial \varepsilon_n^\sigma} \left( \mathbf{e}_i \frac{\partial \varepsilon_n^\sigma(\mathbf{k})}{\partial \mathbf{k}} \right) \left( \mathbf{e}_j \frac{\partial \varepsilon_n^\sigma(\mathbf{k})}{\partial \mathbf{k}} \right).
\end{aligned} \quad (2)
$$

Here, $f(\varepsilon_n^\sigma)$ is the Fermi function for the spin $\sigma$ and band $n$, $V$ is the unit cell volume, $\varepsilon_n^\sigma(\mathbf{k})$ is Kohn-Sham eigenvalue for band $n$, $k$-point $\mathbf{k}$, spin-channel $\sigma$, $\mathbf{e}_i$ is unit vector in $i$ direction, $i = x, y, z$, $\omega_{ij}$ is the total plasma frequency that includes contributions from spin-majority ($\sigma = \uparrow$), and spin-minority ($\sigma = \downarrow$) electrons.

We have implemented the analytic derivatives of the Kohn-Sham eigenvalues with respect to $k$ point in the all-electron full-potential electronic-structure package FHI-aims [20]. The FHI-aims employs numeric atom-centered orbitals (NAO) as basis functions of the general form

$$
\varphi_\alpha(\mathbf{r}) = \frac{u_\alpha(r)}{r} Y_{lm}(\Omega), \quad (3)
$$

where $u_\alpha(r)$ is a numerically tabulated radial part, and $Y_{lm}$ are spherical harmonics. Due to the localized basis functions, core electrons are treated explicitly, without the need for additional approximations. In the case of periodic boundary conditions the Kohn-Sham equations become $\mathbf{k}$ space dependent:

$$
\sum_\beta c_{\beta n}^\sigma(\mathbf{k}) \sum_{\mathbf{R}} (h_{\alpha\beta}^{\sigma\mathbf{R}} - \varepsilon_n^\sigma(\mathbf{k}) s_{\alpha\beta}^{\mathbf{R}}) e^{i k \mathbf{R}} = 0, \quad (4)
$$

where $c_{\beta n}^\sigma(\mathbf{k})$ are k-space dependent Kohn-Sham eigenvectors, and $h_{\alpha\beta}^{\sigma\mathbf{R}}$ and $s_{\alpha\beta}^{\mathbf{R}}$ are real-space Hamiltonian and overlap matrix elements:

$$
h_{\alpha\beta}^{\sigma\mathbf{R}} = \langle \varphi_\alpha^{\mathbf{0}} | \hat{h}_{KS}^\sigma | \varphi_\beta^{\mathbf{R}} \rangle, \; s_{\alpha\beta}^{\mathbf{R}} = \langle \varphi_\alpha^{\mathbf{0}} \mid \varphi_\beta^{\mathbf{R}} \rangle, \quad (5)
$$

where $\mathbf{R}$ is a lattice vector, and $\varphi_\alpha^{\mathbf{R}}(\mathbf{r}) = \varphi_\alpha(\mathbf{r} + \mathbf{R})$.

Taking into account Eq. (4) and wave-function normalization condition, one can show that the terms with $dc_{\alpha n}^\sigma(\mathbf{k})/d\mathbf{k}$ vanish, in analogy with the Hellmann-Feynman theorem (see Fig. S1). The derivative of Kohn-Sham eigenenergy in Eq. (2) is calculated in the following way:

$$
\frac{d\varepsilon_n^\sigma(\mathbf{k})}{d\mathbf{k}} = \sum_{\alpha\beta\mathbf{R}} i\mathbf{R} c_{\alpha n}^{\sigma*}(\mathbf{k}) c_{\beta n}^\sigma(\mathbf{k}) e^{i k \mathbf{R}} [h_{\alpha\beta}^{\sigma\mathbf{R}} - s_{\alpha\beta}^{\mathbf{R}} \varepsilon_n^\sigma(\mathbf{k})], \quad (6)
$$

where $\varepsilon_n^\sigma(\mathbf{k}) = \langle \psi_n^\sigma(\mathbf{k}) \mid \hat{h}_{KS}^\sigma \mid \psi_n^\sigma(\mathbf{k}) \rangle$ and $\psi_n^\sigma(\mathbf{k}) = \sum_\alpha c_{\alpha n}^\sigma(\mathbf{k}) \sum_{\mathbf{R}} e^{i k \mathbf{R}} \varphi_\alpha(\mathbf{r} + \mathbf{R})$ is a Kohn-Sham eigenfunction.

### B. Spin-orbit coupling

The inclusion of spin-orbit coupling (SOC) is particularly important for heavy elements such as gold, silver, palladium, and platinum. For lightweight elements such as aluminium and sodium, SOC effects are expected to be very small. Ambrosch-Draxl [9] reports $\sim 0.2$ eV correction to plasma frequency for bulk gold and $\sim 1.3$ eV for bulk platinum with inclusion of spin-orbit coupling.

In Kohn-Sham DFT the effects of SOC on electronic levels can be incorporated into calculations nonself-consistently by introducing SOC-perturbations to Hamiltonian:

$$\hat{h}_{\text{SOC}} = \hat{h}_{KS} + \hat{v}_{\text{SOC}}, \tag{7}$$

where $\hat{h}_{KS}$ is the Kohn-Sham Hamiltonian operator and $\hat{v}_{\text{SOC}}$ is SOC operator in atomic units,

$$\hat{v}_{\text{SOC}} = \frac{i}{4c^2}\hat{\boldsymbol{\sigma}} \cdot \hat{\boldsymbol{p}}\hat{v} \times \hat{\boldsymbol{p}}. \tag{8}$$

Here, $\hat{\boldsymbol{p}}$ is the momentum operator, and $\hat{\boldsymbol{\sigma}}$ are the Pauli matrices:

$$\hat{\sigma}_x = \begin{bmatrix} 0 & 1 \\ 1 & 0 \end{bmatrix}, \quad \hat{\sigma}_y = \begin{bmatrix} 0 & -i \\ i & 0 \end{bmatrix}, \quad \hat{\sigma}_z = \begin{bmatrix} 1 & 0 \\ 0 & -1 \end{bmatrix}. \tag{9}$$

In the case of the SOC Hamiltonian, the Kohn-Sham eigenvalue derivatives cannot be expressed separately for each spin because the spin-orbit coupling term includes interaction between spin-up and spin-down electrons:

$$\frac{d\varepsilon_n(\mathbf{k})}{d\mathbf{k}} = \sum_{\mathbf{R}} i\mathbf{R}e^{ik\cdot R} \sum_{\alpha,\beta} \left\{ \sum_{\sigma} C_{\alpha n}^{\sigma*}(\mathbf{k})C_{\beta n}^{\sigma}(\mathbf{k})[h_{\alpha\beta}^{\sigma\mathbf{R}} - s_{\alpha\beta}^{\mathbf{R}}\varepsilon_n] + \sum_{\sigma\sigma'} C_{\alpha n}^{\sigma*}(\mathbf{k})C_{\beta n}^{\sigma'}(\mathbf{k})v_{\alpha\beta}^{\sigma\sigma'\mathbf{R}} \right\}. \tag{10}$$

Here $v_{\alpha\beta}^{\sigma\sigma'\mathbf{R}} = \langle \varphi_\alpha^{\mathbf{0}\sigma} | \hat{v}_{\text{SOC}} | \varphi_\beta^{\mathbf{R}\sigma'} \rangle$, where $|\varphi_\alpha^{\mathbf{R}\uparrow}\rangle = |\varphi_\alpha^{\mathbf{R}}, 0\rangle$, $|\varphi_\alpha^{\mathbf{R}\downarrow}\rangle = |0, \varphi_\alpha^{\mathbf{R}}\rangle$ are spinors, $\varepsilon_n$ are SOC-perturbed Kohn-Sham eigenvalues, $C_{n\alpha}^{\sigma}$ are Kohn-Sham eigenfunctions in a basis of diagonalized perturbation matrix:

$$C_{\alpha n}^{\sigma}(\mathbf{k}) = \sum c_{nm}^{\text{soc}}(\mathbf{k})c_{\alpha m}^{\sigma}(\mathbf{k}), \tag{11}$$

where $c_{nm}^{\text{soc}}$ are the coefficients of SOC-perturbed eigenvectors in a basis of the unperturbed eigenvectors $c_{m\alpha}^{\sigma}$. In Eq. (10) the terms with $\partial c_{\alpha n}^{\sigma}(\mathbf{k})/\partial\mathbf{k}$ [coming from Eq. (11)] do not vanish, since $c_{n\alpha}^{\sigma}(\mathbf{k})$ are not eigenvectors of the SOC Hamiltonian in the NAO basis. In general, the perturbation $v_{soc}$ should be small, and the derivative become negligible.

In order to analyze the effect of neglecting $\partial c_{\alpha n}^{\sigma}(\mathbf{k})/\partial\mathbf{k}$, we calculate plasma frequency for a chain of lithium atoms and artificially add large $v_{soc}$, such that $\max\{v_{soc}\} \sim 1$. We calculate the $d\varepsilon_n(\mathbf{k})/d\mathbf{k}$ using the Eq. (10) and compare it to numerically calculated $d\varepsilon_n(\mathbf{k})/d\mathbf{k}$ using fast Fourier transform. In Fig. S1 [21] we show that even for the large perturbation neglecting the term containing $\partial C_{n\alpha}^{\sigma}(\mathbf{k})/\partial\mathbf{k}$ still gives generally correct predictions for the shape and values of the perturbed Kohn-Sham eigenvalue derivatives.

### III. COMPUTATIONAL APPROACH

Plasma frequency of the nine metals (Ag, Al, Au, Cu, Na, Pt, Pd, Co, and Fe) is obtained. DFT calculations are performed using FHI-aims [20] and Vienna *ab initio* simulation package (VASP) [22–25]. FHI-aims employs the numeric atomic orbital basis sets, and therefore core electrons are explicitly included in the calculation, without the need for pseudopotential approximation. "Tight" settings are used to ensure convergence with respect to numerical settings. We employ the generalized gradient approximation in the form of the Perdew, Burke, Ernzerhof (PBE) exchange-correlation functional [6] and the strongly constrained and appropriately normed functional SCAN [19]. Convergence tests with respect to k-point mesh and smearing width are performed. FHI-aims calculations are compared to VASP results. We employ projector-augmented wave (PAW-PBE) pseudopotentials for all metals. The plane-wave energy cutoff is 450 eV for all metals except Na and Al. For Na and Al the cutoff is 500 eV.

Crystal structure of all metals except Na and Fe is face-centered cubic (fcc). Na and Fe have body-centered cubic

(bcc) structure. We also consider two modifications of Co: hexagonal close packed (hcp) and fcc, since both hexagonal and cubic nanoparticles are observed in the study [1]. Calculations are done using primitive cells containing one atom, except for hcp Co, which contains two atoms. Lattice parameters are obtained by atomic relaxation at k-points $41 \times 41 \times 41$ with the respective functional (PBE or SCAN) using FHI-aims. The obtained lattice parameters are then used for plasma frequency calculations in both VASP and FHI-aims.

Electronic structure and density of states are obtained nonself-consistently at the relaxed geometry with $123 \times 123 \times 123$ Γ-centered k-point mesh (see Figs. S2–S8 [21]). For Fe and fcc Co all properties are calculated on k-point grid $93 \times 93 \times 93$. For hcp Co the k-point grid is $93 \times 93 \times 63$. The study of Co and Fe also takes colinear spinpolarization into account (see Figs. S9–S11 [21]). Converging k-grid density is important for accurate calculations of optical properties of metals [14] (see Fig. S12 in SI). For VASP calculations plasma frequencies are calculated on k-grids $64 \times 64 \times 64$ and $65 \times 65 \times 65$ and then averaged. The error for the VASP calculations is $\pm 0.1$ eV, and the error for FHI-aims calculations is $\pm 0.01$ eV because of the denser k-point mesh. Denser k-grids were achieved with FHI-aims due to a more favourable scaling of computational cost with k-grid density.

### IV. RESULTS AND DISCUSSION

Tables I and II summarize properties calculated with FHI-aims and VASP in comparison with experiment. The root-mean-square error (RMSE) for PBE lattice constants is 1.6%, and the RMSE for SCAN lattice constants is 0.6%. Figure 2 shows the correlation between theoretically predicted and experimentally measured plasma frequencies.

Calculated and derived from experiment plasma frequencies are compared with and without inclusion of SOC for PBE and SCAN in Tables I and II. The RMSE for PBE and SCAN plasma frequencies with included SOC are 4.2% and 1.7% respectively. Thus, SCAN consistently improves over PBE and gives rather accurate results for the considered properties of metals.

Cubic and hexagonal metals are highly symmetric which leads to zero off-diagonal elements of the plasma frequency tensor. In cubic crystals $\omega_{xx} = \omega_{yy} = \omega_{zz} = \omega$, however in hexagonal crystals $\omega_{xx} = \omega_{yy} = \omega_1$, but $\omega_{zz} = \omega_2 \neq \omega_1$.

TABLE I. Calculated lattice constants and dielectric properties for metals compared to experimental values. Zero-point vibrational effects are removed from experimental results for lattice constants for a direct comparison with the calculated values [26].

| Metal | | XC functional | Lattice constant, Å | | Plasma frequency, eV | | | |
|---|---|---|---|---|---|---|---|---|
| | | | *ab initio* | Expt. | VASP | FHI-aims | FHI-aims (SOC) | Expt. |
| Al | fcc | PBE | 4.038 | 4.019 | 12.4 | 12.45 | 12.45 | 12.4[16] |
| | | SCAN | 4.014 | | – | 12.53 | 12.53 | |
| Ag | fcc | PBE | 4.140 | 4.063 | 9.0 | 9.00 | 9.00 | 9.2 [10] |
| | | SCAN | 4.041 | | – | 9.48 | 9.47 | |
| Au | fcc | PBE | 4.152 | 4.061 | 8.7 | 8.75 | 8.63 | 9.1 [10] |
| | | SCAN | 4.095 | | – | 9.09 | 8.98 | |
| Cu | fcc | PBE | 3.630 | 3.595 | 8.9 | 8.89 | 8.88 | 9.3 [10] |
| | | SCAN | 3.556 | | – | 9.32 | 9.31 | |
| Na | bcc | PBE | 4.184 | 4.207 | 6.0 | 6.04 | 6.04 | 6.0 [17] |
| | | SCAN | 4.192 | | – | 6.12 | 6.12 | |
| Pd | fcc | PBE | 3.942 | 3.876 | 7.1 | 7.11 | 6.85 | 7.4[2] |
| | | SCAN | 3.891 | | – | 7.52 | 7.30 | |
| Pt | fcc | PBE | 3.966 | 3.913 | 8.5 | 8.53 | 7.20 | |
| | | SCAN | 3.912 | | – | 9.17 | 7.96 | |

In VASP, calculation of linear optical response is not implemented for META-GGA in the used version 5.4.4, therefore we can only compare the results for PBE calculations for VASP and FHI-aims.

As expected, taking into account SOC for such metals as Al, Cu, and Na has a negligible effect on plasma frequency. For Au and Pd the effect of SOC is also small, but not negligible and is around 0.2 eV, which is comparable to the one reported previously [9]. SOC systematically reduces plasma frequency. In Pt it experiences the most dramatic change of 1.3 eV upon inclusion of SOC. The analysis of electronic density of states (DOS) shows that Pt DOS at the Fermi level changes dramatically upon inclusion of SOC, which does not happen with the other metals (see Fig. S8 [21]). This explains the large effect of SOC on plasma frequency in Pt, since according to Eq. (2), the largest contribution to plasma frequency comes from electrons around the Fermi level. The complexity of extracting plasma frequency from experiment for Pt arises from the significant interband contribution at low frequencies for this metal [9]. Currently there is no reliable experimental value.

As can be seen from Table II, for hcp Co the contribution to plasma frequency from spin-majority ($\omega_{xx,\uparrow}$) and spin-minority ($\omega_{xx,\downarrow}$) electrons differ by ~1.6 eV, which is comparable to the whole visible range of 2 eV. The total $\omega_{pl}$ is 1 eV different from the value for a majority electrons. $\omega_{zz,\uparrow}$ and $\omega_{zz,\downarrow}$ are almost identical and thus resulting in total plasma frequency $\sim\sqrt{2}\omega_{pl,\uparrow}$. For fcc Co, $\omega_{\uparrow}$ and $\omega_{\downarrow}$ are also almost identical. For the bcc Fe, however, the spin-majority contribution to plasma frequency is around 1.5 times higher than the spin-minority one.

There is a significant difference of the DOS at the Fermi level for the two spin channels for spin-polarized metals (see Figs. S9–S11 [21]). Although DOS at the Fermi level is larger in the spin-minority channel, the corresponding contribution to plasma frequency is smaller. This is because the group velocity is higher in the spin-majority channel due to the higher electron density.

The inclusion of SOC has a relatively large effect of 0.14 eV for bcc Fe and fcc Co. Interestingly, hexagonal Co experiences an even more drastic change of 0.5 eV for its $z$-component plasma frequency $\omega_{zz}$ that decreases from 6.73

TABLE II. Lattice constants and plasma frequencies for hcp and fcc Co and bcc Fe, calculated with FHI-aims and compared to experimental values. Zero-point vibrational effects are removed from experimental results for lattice constants for a direct comparison with the calculated values. Plasma frequencies squared are calculated separately for majority and minority electrons and then summed up to give the total value of plasma frequency squared. The respective values for hcp structure are represented as $\omega_{xx}/\omega_{zz}$. SOC-perturbed plasma frequency is denoted $\omega_{pl}^{soc}$.

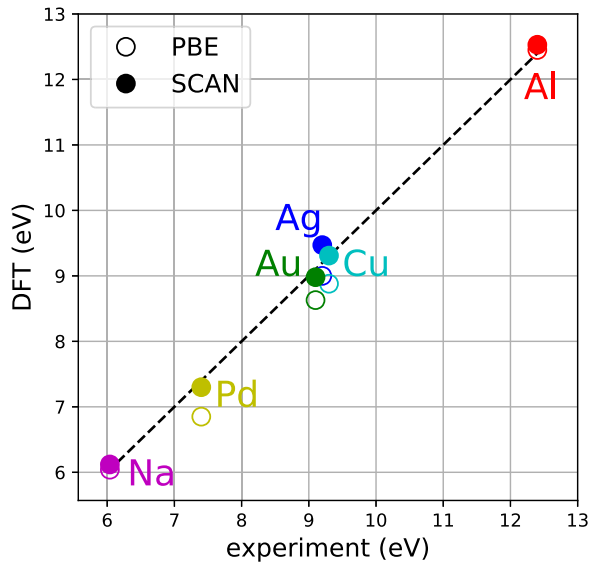| Metal | Lattice constant, A | | | | plasma frequency, eV | | | |
|---|---|---|---|---|---|---|---|---|
| | *ab initio* | | Expt. | | $\omega_{pl,\uparrow}$ | $\omega_{pl,\downarrow}$ | $\omega_{pl}$ | $\omega_{pl}^{soc}$ |
| | a | c | a | c | $\omega_{xx,\uparrow}/\omega_{zz,\uparrow}$ | $\omega_{xx,\downarrow}/\omega_{zz,\downarrow}$ | $\omega_{xx}/\omega_{zz}$ | $\omega_{xx}^{soc}/\omega_{zz}^{soc}$ |
| Fe-bcc | 2.818 | – | 2.855 | – | 5.57 | 3.72 | 6.70 | 6.56 |
| Co-fcc | 3.513 | – | 3.543 | – | 5.44 | 5.05 | 7.42 | 7.28 |
| Co-hcp | 2.493 | 4.033 | 2.503 | 4.057 | 5.03/4.89 | 3.44/4.63 | 6.09/6.73 | 6.01/6.24 |

FIG. 2. Correlation between theoretically predicted and experimentally derived plasma frequencies. *x*-axis value is experimental plasma frequencies in eV. *y* axis shows plasma frequency values calculated from DFT. Open circles are for PBE results, closed circles are for SCAN. The black line is the line where theoretical and experimental data would coincide. Each metal is represented with the respective color (e.g., gold with green, silver with blue, copper with cyan, etc.).

to 6.24 eV. This demonstrates that effects of SOC on calculated optical properties of metals are determined not only by the species but also by the crystal structure. $\omega_{xx}$ does not change much (from 6.09 to 6.01 eV) with the inclusion of SOC.

## V. CONCLUSIONS

A methodology to calculate plasma frequency in an all-electron full-potential framework employing numeric atomic orbital basis sets, including spin-orbit coupling effects, is introduced. Lattice constants and plasma frequency for seven nonmagnetic metals and two ferromagnetic metals are calculated using PBE and SCAN DFT approximations. A good agreement of the obtained results with experiments is achieved, in particular with SCAN. A very large effect of SOC on plasma frequency is obtained for Pt (reduction by 1.2 eV). Also, we find a large effect of crystal structure on the SOC correction to plasma frequency for Co.

Using the new implementation, contributions to the plasma frequency from different spin channels are calculated and analyzed. We find a large difference between calculated contributions from majority and minority electrons to plasma frequency of Co and Fe. The obtained difference for hexagonal close-packed Co reaches 1.6 eV, which is comparable to the whole visible range. Thus, spin-polarization effects on electronic structure can have a significant contribution to the optical spectra of magnetic metal nanoparticles.

[1] H. L. Bhatta, A. E. Aliev, and V. P. Drachev, New mechanism of plasmons specific for spin-polarized nanoparticles, Sci. Rep. **9**, 1 (2019).

[2] P. Johnson and R. Christy, Optical constants of transition metals: Ti, v, cr, mn, fe, co, ni, and pd, Phys. Rev. B **9**, 5056 (1974).

[3] D. M. Ceperley and B. J. Alder, Ground State of the Electron Gas By a Stochastic Method, Phys. Rev. Lett. **45**, 566 (1980).

[4] J. P. Perdew, E. R. McMullen, and A. Zunger, Density-functional theory of the correlation energy in atoms and ions: a simple analytic model and a challenge, Phys. Rev. A **23**, 2785 (1981).

[5] B. S. Mendoza and W. L. Mochán, Ab initio theory of the drude plasma frequency, J. Opt. Soc. Am. B **38**, 1918 (2021).

[6] J. P. Perdew, K. Burke, and M. Ernzerhof, Generalized Gradient Approximation Made Simple, Phys. Rev. Lett. **77**, 3865 (1996).

[7] S. Laref, J. Cao, A. Asaduzzaman, K. Runge, P. Deymier, R. W. Ziolkowski, M. Miyawaki, and K. Muralidharan, Size-dependent permittivity and intrinsic optical anisotropy of nanometric gold thin films: A density functional theory study, Opt. Express **21**, 11827 (2013).

[8] J. Harl, The linear response function in density functional theory, Ph.D. thesis, Uniwien, 2008.

[9] K. Glantschnig and C. Ambrosch-Draxl, Relativistic effects on the linear optical properties of au, pt, pb and w, New J. Phys. **12**, 103048 (2010).

[10] P. B. Johnson and R. Christy, Optical constants of the noble metals, Phys. Rev. B **6**, 4370 (1972).

[11] A. Marini, R. Del Sole, and G. Onida, First-principles calculation of the plasmon resonance and of the reflectance spectrum of silver in the gw approximation, Phys. Rev. B **66**, 115101 (2002).

[12] Y. He and T. Zeng, First-principles study and model of dielectric functions of silver nanoparticles, J. Phys. Chem. C **114**, 18023 (2010).

[13] A. Marini, G. Onida, and R. Del Sole, Plane-wave dft-lda calculation of the electronic structure and absorption spectrum of copper, Phys. Rev. B **64**, 195125 (2001).

[14] C. Ambrosch-Draxl and J. O. Sofo, Linear optical properties of solids within the full-potential linearized augmented planewave method, Comput. Phys. Commun. **175**, 1 (2006).

[15] D. Y. Smith and B. Segall, Intraband and interband processes in the infrared spectrum of metallic aluminum, Phys. Rev. B **34**, 5191 (1986).

[16] H. Ehrenreich, H. Philipp, and B. Segall, Optical properties of aluminum, Phys. Rev. **132**, 1918 (1963).

[17] M. Haque and K. Kliewer, Plasmon properties in bcc potassium and sodium, Phys. Rev. B **7**, 2416 (1973).

[18] N. Matsko, Formation of normal surface plasmon modes in small sodium nanoparticles, Phys. Chem. Chem. Phys. **22**, 13285 (2020).

[19] J. Sun, A. Ruzsinszky, and J. P. Perdew, Strongly Constrained and Appropriately Normed Semilocal Density Functional, Phys. Rev. Lett. **115**, 036402 (2015).

[20] V. Blum, R. Gehrke, F. Hanke, P. Havu, V. Havu, X. Ren, K. Reuter, and M. Scheffler, Ab initio molecular simulations with numeric atom-centered orbitals, Comput. Phys. Commun. **180**, 2175 (2009).

[21] See Supplemental Material at http://link.aps.org/supplemental/ 10.1103/PhysRevB.107.045113 for the derivation of Kohn-Sham eigenenergy derivatives and Figs. S1– S12.

[22] G. Kresse and J. Hafner, Ab initio molecular-dynamics simulation of the liquid-metal–amorphous-semiconductor transition in germanium, Phys. Rev. B **49**, 14251 (1994).

[23] G. Kresse and J. Furthmüller, Efficient iterative schemes for ab initio total-energy calculations using a plane-wave basis set, Phys. Rev. B **54**, 11169 (1996).

[24] G. Kresse and J. Furthmüller, Efficiency of ab-initio total energy calculations for metals and semiconductors using a plane-wave basis set, Comput. Mater. Sci. **6**, 15 (1996).

[25] G. Kresse and D. Joubert, From ultrasoft pseudopotentials to the projector augmented-wave method, Phys. Rev. B **59**, 1758 (1999).

[26] P. Hao, Y. Fang, J. Sun, G. I. Csonka, P. H. T. Philipsen, and J. P. Perdew, Lattice constants from semilocal density functionals with zero-point phonon correction, Phys. Rev. B **85**, 014111 (2012).